STATISTICAL PROPERTIES OF THE PHASE DIFFERENCE BETWEEN THE SOUND PRESSURE AND PARTICLE VELOCITY

VLADIMIR SHCHUROV, VLADIMIR KOULESHOV, MARIANNA KUYANOVA, HELEN TKACHENKO

V.I. Il'ichev Pacific Oceanological Institute
690041, 43, Baltiyskaya St., Vladivostok, Russia
shchurov@poi.dvo.ru

The paper is focused on statistical properties of time derivative of the phase difference between pressure and particle velocity orthogonal projections in the acoustic field composed of a tone or noise-shaped signal and underwater ambient noise in different proportions. The paper does not relate phase difference measurements with oceanological properties of the medium. The paper presents measurements made in shallow water and deep open ocean, and with different proportions between noise and signal. When the exponent averaging time is taken greater than 1 s, mean values of time derivatives approximate zero with different probability densities in different frequency bands.

INTRODUCTION

Much progress toward solving practical problems in underwater acoustics depends on completeness of the information available on the acoustic field of interest. Traditionally, such information is acquired by means of lengthy hydrophone arrays. However, adequate acoustic data can be derived from measurements made by a single combined sensor placed at a given point. Combined sensor at a single point in the wave field makes simultaneous measurements of a sound pressure $p(t)$ and three orthogonal projections of the particle velocity vector $\vec{V}(t)$ $\{V_x(t),\ V_y(t),\ V_z(t)\}$, and, consequently, phase-difference and correlation relationships between them. It is known that in arbitrary determined harmonic acoustic field formed by a single source and a plane wave, the pressure and the particle velocity are in phase, i.e. phase difference is zero. When a number of sources of the same frequency are found, nonzero phase differences, $\Delta\varphi_x=\varphi_p-\varphi_x$, $\Delta\varphi_y=\varphi_p-\varphi_y$, $\Delta\varphi_z=\varphi_p-\varphi_z$, exist, where:

$$
\begin{aligned}
&p(t) = p_0 \cos(\omega t + \varphi_p),\\
&V_x(t) = V_{0,x} \cos(\omega t + \varphi_p - \varphi_x),\\
&V_y(t) = V_{0,y} \cos(\omega t + \varphi_p - \varphi_y),\\
&V_z(t) = V_{0,z} \cos(\omega t + \varphi_p - \varphi_z),\\
&\vec{V} = \vec{i}\,V_x + \vec{j}\,V_y + \vec{k}\,V_z \qquad (\vec{i},\vec{j},\vec{k} \text{ - unit orthogonal vectors})
\end{aligned} \tag{1}
$$

In general case the particle velocity vector $\vec{V}(t)$ draws an ellipse in one oscillation period [1]. In that case $\vec{V}(t)$ vector and the wave propagation do not coincide. In determined acoustic field $\Delta\varphi_x=\varphi_p - \varphi_x$, $\Delta\varphi_y=\varphi_p - \varphi_y$, $\Delta\varphi_z=\varphi_p - \varphi_z$ are time-independent that permits active, $\vec{V}_a(t)$, and reactive, $\vec{V}_r(t)$, particle velocity components being introduced, as well as the active intensity vector (the Umov' vector), $\vec{I}_a$, and reactive intensity vector, $\vec{I}_r$. When $\vec{I}_r = 0$ medium particles move along $\vec{I}_a$ direction. Here traveling wave conditions are satisfied resulting in equal phases of the medium particle velocity and pressure. Above-described characteristics of determined harmonic field can be successfully applied to describe signals present in actual random acoustic fields when tone level is much higher than that of the noise, i.e. signal-to-noise ratio is greater than unit, $SNR>1$. However, in solving practical problems in actual acoustic field, the case of $SNR\leq 1$ is of our prime interest. Actual underwater sound field is a sum of random diffusive field (in which no net energy transport exists) and coherent one (in which net energy transport is to be found) [2]. When acoustic energy reaches the measurement point via several different paths, the instant net pressure is a scalar sum of instant partial pressures. On the other hand, net particle velocity will be a vector sum and depend on each ray angle of arrival. Hence, each item will contribute its specific phase shift relative to corresponding pressure item. This results in net phase shift between net acoustic pressure and particle velocity, being a random quantity. Generally, a signal arrived at the measurement point can be considered as a sum of determined and random parts. In that case the phase difference $\Delta\varphi_i(f)$ $(i=x,y,z)$ is the Fourier transform of data series $p(t)$, $V_x(t)$, $V_y(t)$, $V_z(t)$ recorded in random acoustic field.

$$
\begin{aligned}
&S_{pV_i}(f) = \left|S_{pV_i}(f)\right| e^{-j\Delta\varphi_i(f)}\\
&\Delta\varphi_i(f) = arctn\frac{\mathrm{Im}\,S_{pV_i}(f)}{\mathrm{Re}\,S_{pV_i}(f)}, \text{ where } (i=x,y,z)
\end{aligned} \tag{2}
$$

As field trails carried out in different parts of the Earth Ocean show [3], diffusive noise contribution to cross spectra $S_{pV_i}(f)$, $(i=x,y,z)$ can be completely excluded. Then, within the framework of data processing technique applied, the coherent noise remains the principle trouble.

In determined harmonic process, Eq. 1, the phase differences $\Delta\varphi_x$, $\Delta\varphi_y$, $\Delta\varphi_z$ are constants at a given point in the acoustic field, whereas in the steady ergodic random process these quantities are random, and precisely determine statistical properties of orthogonal projections of the acoustic field energy flux vector, $I_x(f, t)$, $I_y(f, t)$, $I_z(f, t)$, [3]. This is just the point that explains the interest in statistical properties of $\Delta\varphi_x(f, t)$, $\Delta\varphi_y(f, t)$, $\Delta\varphi_z(f, t)$. The paper analyses phase difference behavior using field trails processing results. Actual acoustic fields of interest consist of signal and noise in different proportions.

1. FIELD TRAIL SETTING

Shallow water experiment technique was as follows. Bottom combined sensing system including a sound pressure sensor (scalar sensor) and three-component particle velocity sensor (vector sensor) was placed at the depth of 30 m 300 m off shore. Combined sensor of the sensing system was 1.5 m above sludgy sea bed. Its *x*- and *y*-axes were in the horizontal plane with *x*-axis directed to the shore; z-axis was pointed downward. The measurement point was 10 km away from the shore. Wind speed was less than 2 m/s, surface waves were low. Working frequency band was 20 to 1000 Hz. The tone source was 20 m deep 2 km apart from the sensing system with azimuth of 30 deg. Measurement site depth was 80 m. Shipping noise-like signal excess over the ambient noise background in the $S_{p^2}(t)$ autospectrum at f_1=440 Hz was zero, whereas at f_2=501 Hz and f_3=630 Hz (tone frequency) was 3 to 6 dB.

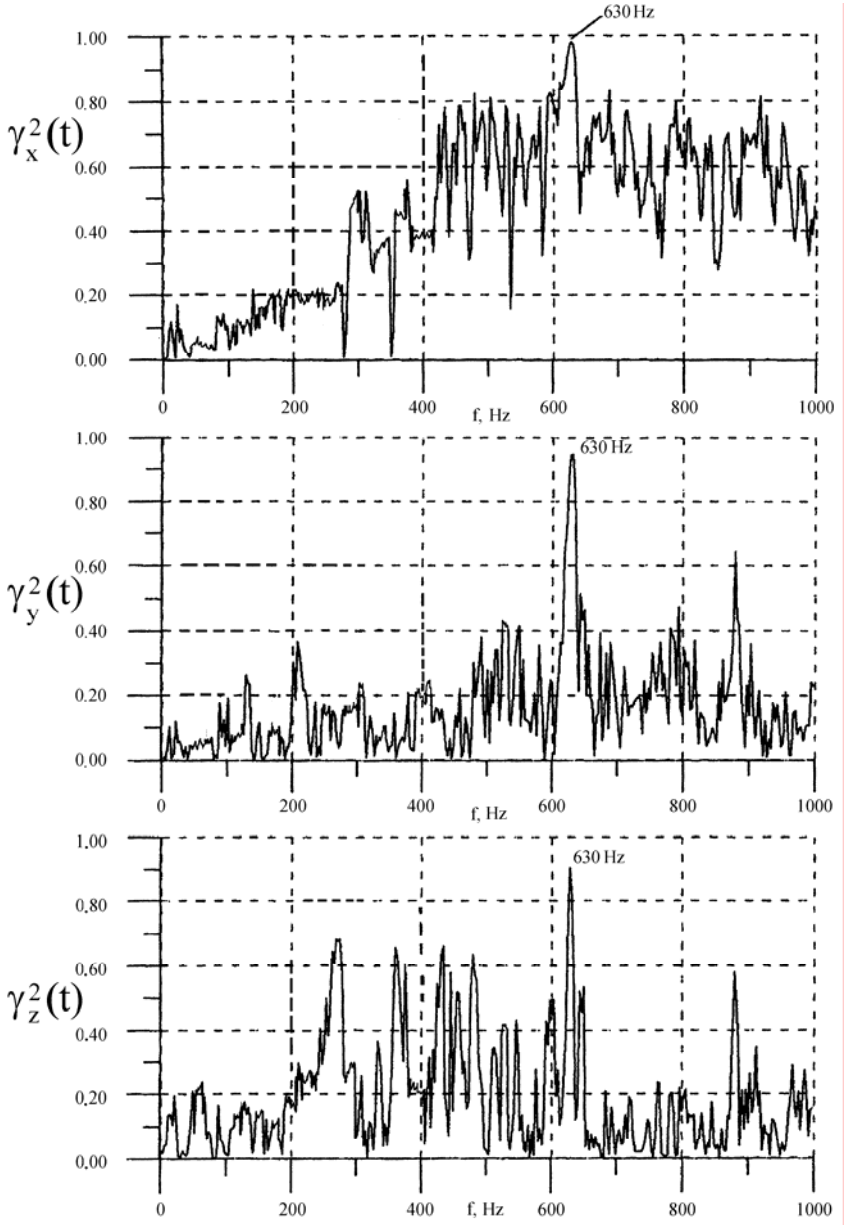

Fig.1 The coherence functions $\gamma_x^2(f)$, $\gamma_y^2(f)$, $\gamma_z^2(f)$. Averaging time is 30 s

Fig. 1 shows the coherence functions, $\gamma_x^2(f)$, $\gamma_y^2(f)$, $\gamma_z^2(f)$, which completely characterize acoustic noise conditions at measurement instant. As seen from Fig. 1, the ambient noise field is anisotropic in the horizontal plane.

Comparison between $\gamma_x^2(f)$ and $\gamma_z^2(f)$, as well as $\gamma_y^2(f)$ and $\gamma_z^2(f)$ evidences that the noise field is also anisotropic in the vertical planes *xy* and *yz*. In the *x*-direction above 400 Hz the ambient noise coherence runs up to 0.8. In *y*- and *z*-directions the coherence is far less. The tone coherence much prevails that of the noise in each of *x*-, *y*-, *z*- directions. That is, in each of *x*-, *y*-, *z*- directions there are broadband coherent shipping noise and tone in different proportions.

The paper also reports results of deep-ocean experiment done in the Sea of Philippine, 18°56′N 129°19′E. The phase-difference relationships $\Delta\varphi_i(t)$ (i=x,y,z) are considered using Lloyd mirror curve of the 404-Hz tone. Depth of the source was 60 m, the measurement point depth 530 m. Sound speed at the surface was greater than that at the bottom. The underwater sound channel axis was 1000 m deep. Near-surface wind speed was less than 2 m/s, low waves with swell.

2. DATA PROCESSING

Statistical properties of phase difference time derivatives are considered:

$$\varepsilon_x = \frac{d\left(\Delta\varphi_x(t)\right)}{dt}, \qquad \varepsilon_y = \frac{d\left(\Delta\varphi_y(t)\right)}{dt}, \qquad \varepsilon_z = \frac{d\left(\Delta\varphi_z(t)\right)}{dt}. \qquad (3)$$

As stated above, the phase differences $\Delta\varphi_i(t)$ (i=x,y,z) are calculated via Fourier transformation. Experimental data processing was as follows. The pairs $p(t)$, $V_x(t)$; $p(t)$, $V_y(t)$; $p(t)$, $V_z(t)$ were used to compute cross-spectral densities $S_{pV_x}(f,T)$, $S_{pV_y}(f,T)$, $S_{pV_z}(f,T)$ and phase spectra $\Delta\varphi_x(f,T)$, $\Delta\varphi_y(f,T)$, $\Delta\varphi_z(f,T)$ at different times of exponent averaging in the 20 to 1000 Hz frequency band. Averaging times were taken, T=1, 2, 3, 5, 10, 15 s. Then at f_1= 440 Hz, f_2= 501 Hz, and f_3=630 Hz in a number of different bands B_0 = 6, 12, 24 Hz random quantities $\Delta\varphi_i(B_0, T)$ (i=x,y,z) were calculated. Then $\Delta(\Delta\varphi_i(t_1)) = \Delta\varphi_i(t_2) - \Delta\varphi_i(t_1)$ were calculated at $\Delta t = t_2 - t_1$ in each band B_0. As the quantities are rather small, substitutions $\Delta(\Delta\varphi_i(t)) = d(\Delta\varphi_i)$ and $\Delta t = dt$ would be reasonable. Hence, a body of random values $\varepsilon_i = d(\Delta\varphi_i(t))/dt$ (i=x,y,z) was produced.

Statistical analysis of ε_i, (i=x,y,z) was as follows:

1. Probability density histograms $\rho_{i,1,2,3}$ were built as a function of $\sqrt{B_0 T}$ at three frequencies f_1, f_2, f_3 (i=x,y,z).

2. The means $<\varepsilon_{i,1,2,3}>=\left\langle \frac{d(\Delta\varphi_i(t))}{dt} \right\rangle_{1,2,3}$ were calculated as a function of $\sqrt{B_0 T}$.

3. The standard deviations $\sigma_{i,1,2,3}$ were calculated as a function of $\sqrt{B_0 T}$.

4. Probability densities of the means $\rho_{i,1}$, $\rho_{i,2}$, $\rho_{i,3}$ were calculated as a function of $\sqrt{B_0 T}$ (i=x,y,z).

Lloyd mirror curves were built as follows:

1. Autospectra $S_{p^2}(f)$, $S_{V_x^2}(f)$, $S_{V_y^2}(f)$, $S_{V_z^2}(f)$ and cross-spectra $S_{pV_x}(f)$, $S_{pV_y}(f)$, $S_{pV_z}(f)$ were produced using Fourier transformation routine and exponent averaging.

2. At averaging time of 3 s in B_0=5 Hz frequency band about 404 Hz spectral density envelope time-dependences were built, $S_{V_x^2}(f_0,t)$, $S_{V_y^2}(f_0,t)$, $S_{V_z^2}(f_0,t)$. Time series used were 4500 s long.

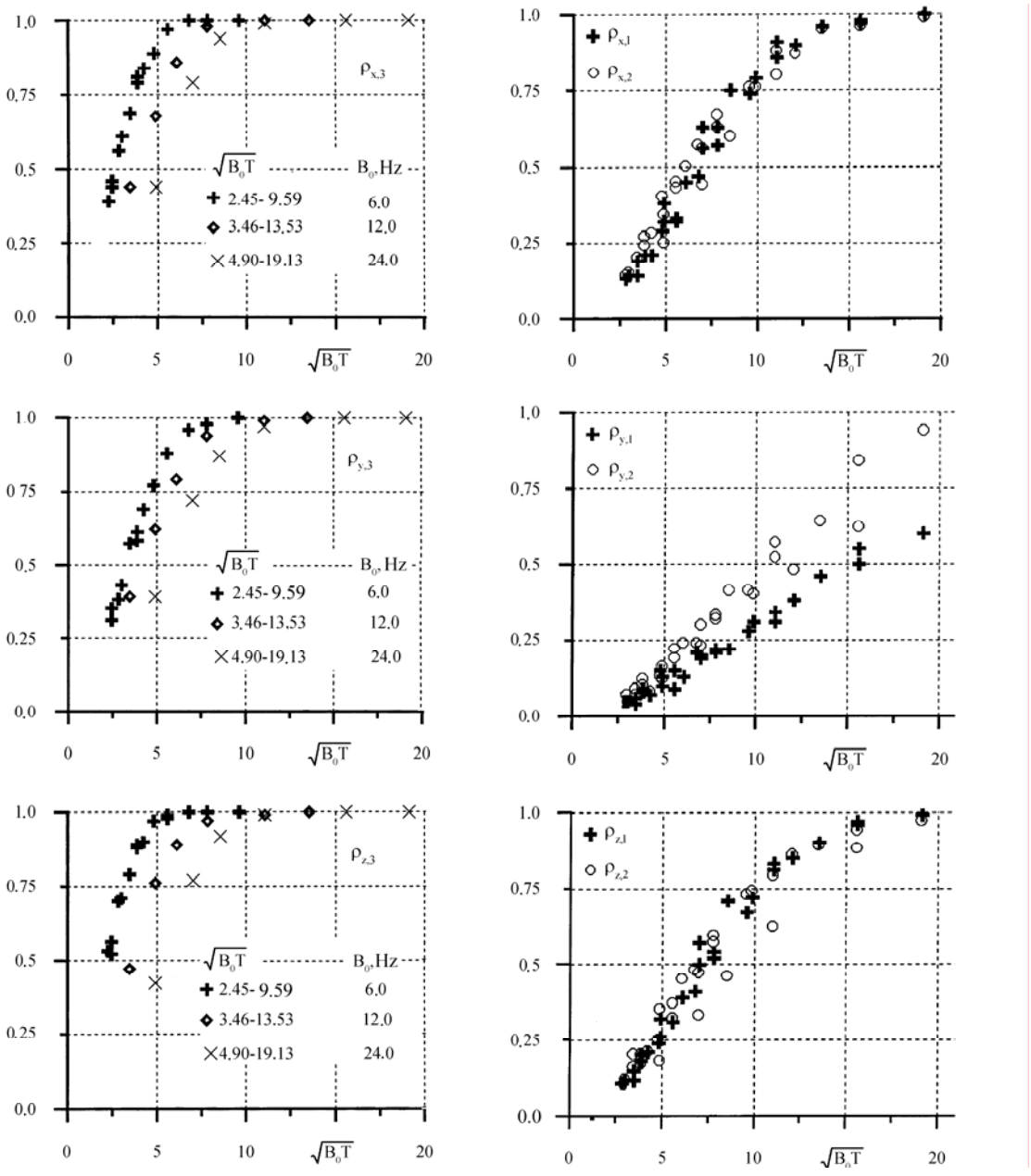

Fig.2 The probability densities $\rho_{i1,2,3}$ of the means $<\varepsilon_{i,1,2,3}>$ (i=x,y,z) as a functions of $\sqrt{B_0T}$; a) – the tone at f_3 = 630 Hz; b) – the noise-shaped signals at f_1 = 440 Hz and f_2 = 501 Hz

3. Envelope time-dependencies were as well built at 540 Hz for the noise from passing by ship.

4. The Eq. 2 was used to build phase difference sonograms $\Delta\varphi_x(f)$, $\Delta\varphi_y(f)$, $\Delta\varphi_z(f)$ in 5-Hz frequency band about 404 and 540 Hz.

3. THE RESULTS

Tab. 1 and Figs. 1,2 present the principle results of shallow water research. Time-derivatives in the Eq. 3 are measured in deg per second alike circular frequency. The derivative here measures velocity of the phase difference change. At three frequencies, f_1, f_2, f_3, the following statistical characteristics were considered as a function of $\sqrt{B_0T}$: the mean derivative, $<\varepsilon_{i,1,2,3}>$; the standard deviation, $\sigma_{i,1,2,3}$; and the mean derivative probability density, $\rho_{i,1,2,3}$; where $i=x,y,z$, B_0 – the frequency bin used, B_0 = 6, 12, 24 Hz, T – the exponent averaging time, T = 1,2,3,5,10,15 s. The quantities $<\varepsilon_{i,1,2,3}>$ and $\sigma_{i,1,2,3}$ are considered as random functions of $\sqrt{B_0T}$.

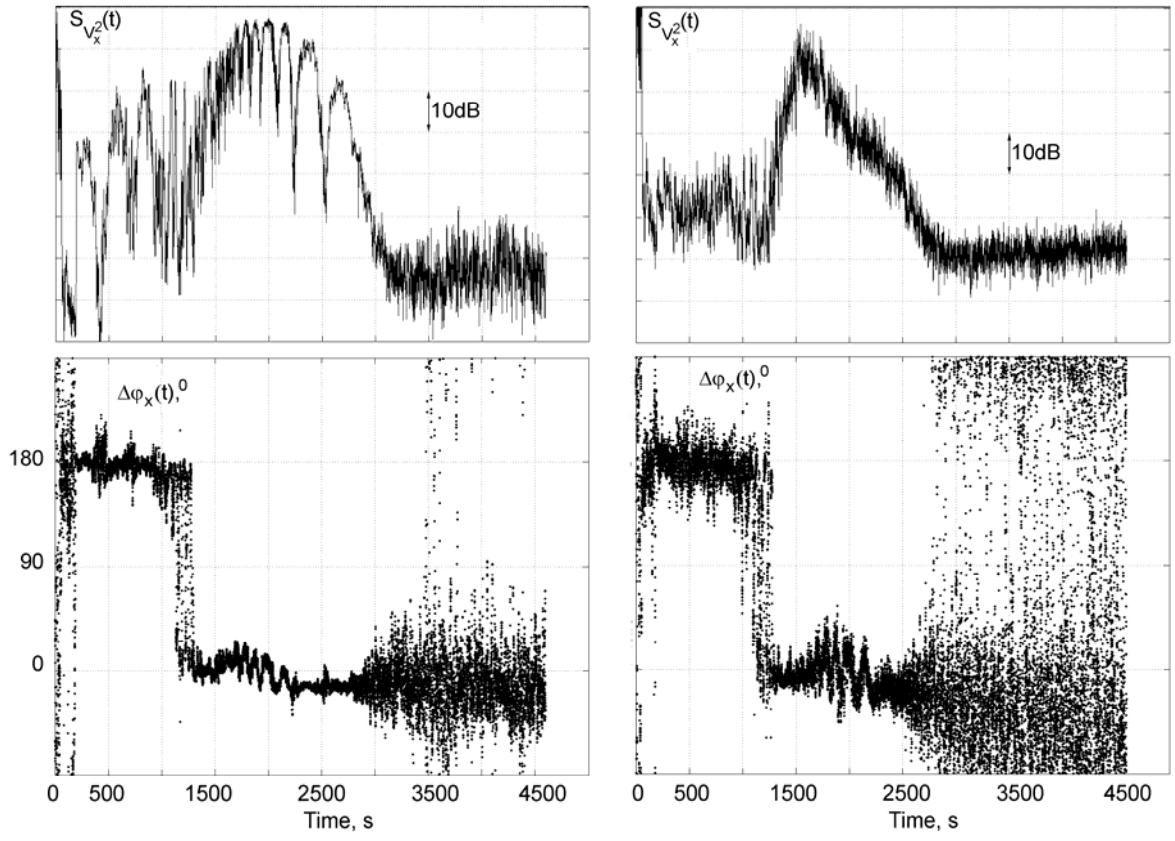

Fig.3 Time-dependence of a) – the envelope of $S_{V_x^2}(f_0,t)$ and phase difference $\Delta\varphi_x(t)$ for the 404-Hz tone (Lloyd mirror); b) - $S_{V_x^2}(f_0,t)$ and $\Delta\varphi_x(t)$ for the noise-shaped signal at 540 Hz. Frequency bin is 5 Hz, time of exponent averaging is 3 s

The tone $<\varepsilon_{i,3}>$ possess the following special features. At averaging times $T \geq 2$ s and B_0 = 6, 12, 24 Hz each of $<\varepsilon_{i,3}>$ is zero within 0.1 deg/s. The standard deviations $\sigma_{i,3}$ depend alike on $\sqrt{B_0 T}$ in all frequency bands decreasing from 1.54 rad/s (at T=1 s and B_0 = 6 Hz) to 0.10 rad/s (at T=15 s and B_0 = 24 Hz) that causes $\rho_{i,3}$ to increase, see Tab. 1. At B_0 = 6 Hz and $\sqrt{B_0 T}$ =5 the probability density $\rho_{x,3} = \rho_{z,3} = 1$ and $\rho_{y,3} = 0.8$. The increase in B_0 to 12 or 24 Hz produces significant decrease in $\rho_{i,3}$ at $\sqrt{B_0 T} \leq 5$; however at $\sqrt{B_0 T} = 10$ the probability densities run to unit. Hence, using B_0 = 6 Hz one can detect random tone against the noise background at averaging time of 1 to 2 s. As for the noise-shaped signal, at both f_1 and f_2 and B_0 = 24 Hz but $<\varepsilon_{x,1,2}>$ is zero, at the same time $\sigma_{i,1,2}$ grows from 2.14 deg/s (T=2 s) to 0.30 deg/s (T=15 s); $\rho_{x,1,2}$ reaches unit at $\sqrt{B_0 T}$ =20. In z-direction $\rho_{z,1,2}$ is also unit at $\sqrt{B_0 T}$ =20, with $<\varepsilon_{z,1}> = 0$ ($T \geq 2$ s) and $<\varepsilon_{z,2}> \neq 0$. In y-direction $\rho_{y,1,2} < 1$ even at $\sqrt{B_0 T}$ =30. Anyway, in the case of broadband signal the increase in frequency bin will tend $<\varepsilon_{i,1,2}>$ to zero with significant decrease in $\sigma_{i,1,2,3}$.

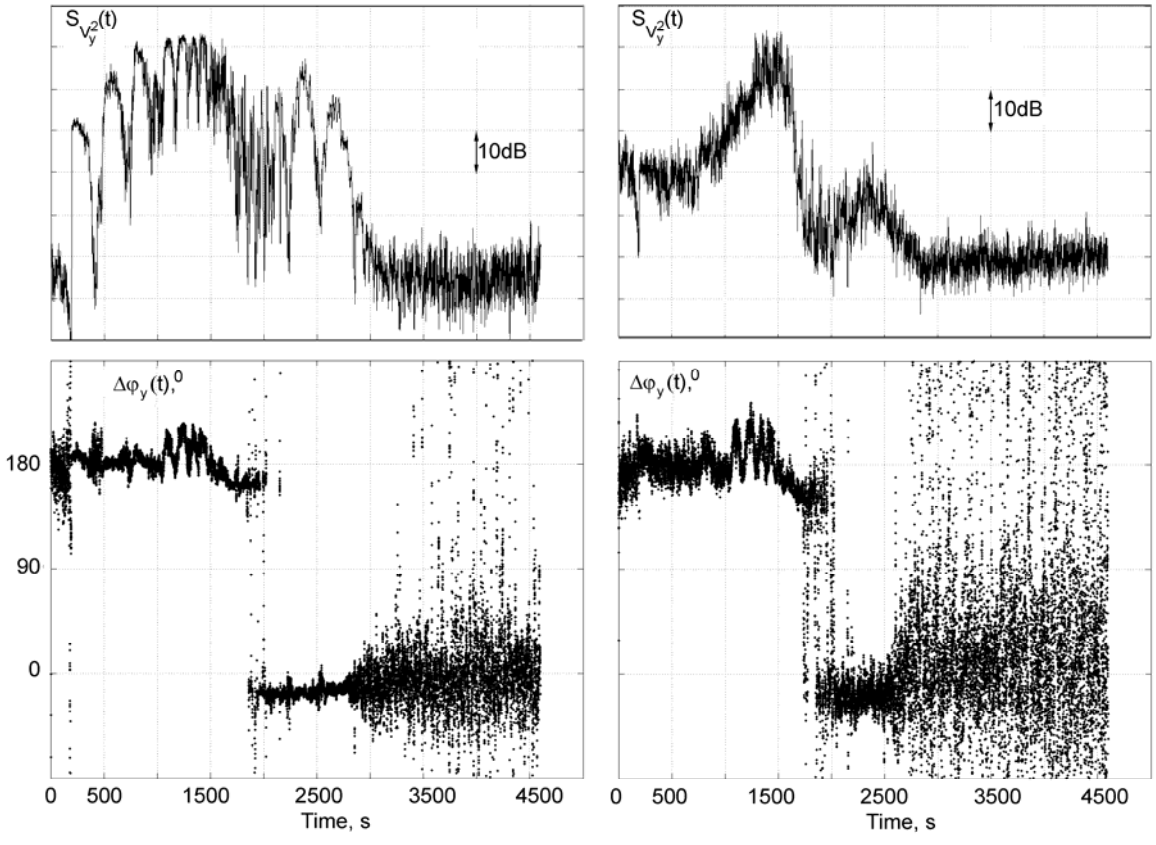

Fig.4 The $S_{V_y^2}(f_0, t)$ and $\Delta\varphi_y(t)$ as a function of time: a) f_0=404 Hz; b) f_0=540 Hz

Smallness of derivative means points to constant phase difference impact or its minor time-dependence in actual random sound field. In the tone case this feature of the phase difference $\Delta\varphi_i(f)$ shows itself even at small averaging times. Discuss the experiment in which

tone excess over the noise background changes much from SNR>>1 to SNR<1. Consider deep-sea trail results recorded by a single combined sensor; Lloyd mirror curves are built for 404-Hz tone and noise-shaped signal at 540 Hz. Figs. 3a-5a illustrate time dependence of envelope of the 404-Hz tone (Lloyd mirror) and corresponding phase difference sonograms $\Delta\varphi_i(t)$, $i=x,y,z$. Figs. 3b-5b show time dependence of the noise envelope of the vessel towing the 404-Hz source at 540 Hz and corresponding phase-difference sonograms at the same frequency.

Envelopes of the spectra $S_{V_x^2}(f_0,t)$, $S_{V_y^2}(f_0,t)$ $S_{V_z^2}(f_0,t)$ are calculated in the 5-Hz frequency bin; time of exponent averaging is 3 s. Phase differences $\Delta\varphi_x(t)$, $\Delta\varphi_y(t)$, $\Delta\varphi_z(t)$ are computed from Eq. 2. The SNR>1 until 300 s. In the 0 to 300 s time interval the phase differences $\Delta\varphi_x(t)$, $\Delta\varphi_y(t)$, $\Delta\varphi_z(t)$ observed are steady close to 0 or 180 deg at 404 Hz as well as 540 Hz. Figs. 3a,b and 4a,b show 180-deg flip in $\Delta\varphi_x(t)$ at about 1200 s, and in $\Delta\varphi_y(t)$ at about 2000 s. This is due to ship crossing the beampattern minimum, *x*-channel at 1200 s and *y*-channel at 2000 s.

No Lloyd Mirror is observed for envelopes of the vessel noise components, $S_{V_x^2}(f_0,t)$, $S_{V_y^2}(f_0,t)$, $S_{V_z^2}(f_0,t)$, since it is on-water noise source here, see Figs. 3b-5b. The 180-deg flips are as well seen in $\Delta\varphi_x(t)$ and $\Delta\varphi_y(t)$ sonograms, Figs.3b, 4b.

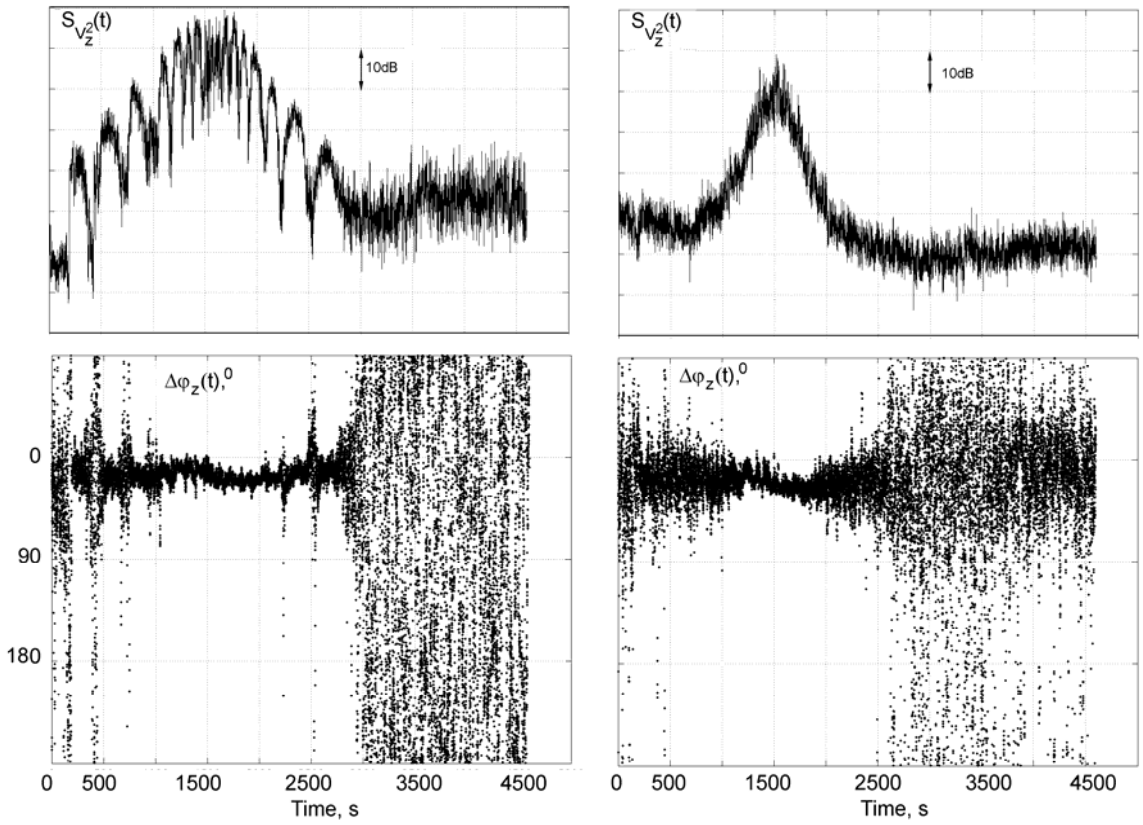

a) b)

Fig.5 The $S_{V_z^2}(f_0,t)$ and $\Delta\varphi_z(t)$ as a function of time; a) f_0=404 Hz, b) f_0=540 Hz

Tab.1 Statistical analysis results for x-, y-, z-channels at f_1 , f_2 , f_3 and frequency intervals B_0=6, 12, 24 Hz, T=1, 2, 3, 5, 10, 15 s

T, s	B_0, Hz	X - channel						Y - channel						Z - channel					
		f_1 = 440 Hz		f_2 = 501 Hz		f_3 = 630 Hz		f_1 = 440 Hz		f_2 = 501 Hz		f_3 = 630 Hz		f_1 = 440 Hz		f_2 = 501 Hz		f_3 = 630 Hz	
		$<\varepsilon_{x,1}>$ deg/s	$\sigma_{x,1}$, deg/s	$<\varepsilon_{x,2}>$ deg/s	$\sigma_{x,2}$, deg/s	$<\varepsilon_{x,3}>$ deg/s	$\sigma_{x,3}$, deg/s	$<\varepsilon_{y,1}>$ deg/s	$\sigma_{y,1}$, deg/s	$<\varepsilon_{y,2}>$ deg/s	$\sigma_{y,2}$, deg/s	$<\varepsilon_{y,3}>$ deg/s	$\sigma_{y,3}$, deg/s	$<\varepsilon_{z,1}>$ deg/s	$\sigma_{z,1}$, deg/s	$<\varepsilon_{z,2}>$ deg/s	$\sigma_{z,2}$, deg/s	$<\varepsilon_{z,3}>$ deg/s	$\sigma_{z,3}$, deg/s
1	6	-1.02	20.36	0.54	14.77	0.24	2.61	-2.17	55.53	1.07	50.68	0.10	3.36	1.15	19.05	0.76	21.14	-0.07	2.25
2	6	-0.25	7.72	0.41	7.78	0.03	1.33	2.69	36.40	1.65	35.00	0.00	1.64	0.40	8.57	0.29	11.64	0.01	0.96
3	6	-0.05	5.09	0.18	5.14	0.01	0.83	2.63	26.47	-1.71	32.80	-0.02	1.10	0.23	5.59	0.16	7.63	0.01	0.64
5	6	-0.03	2.99	0.31	3.63	0.00	0.45	2.90	20.60	-0.12	16.03	-0.02	0.67	0.16	3.26	0.24	4.23	0.02	0.36
10	6	0.02	1.65	0.26	2.83	0.00	0.22	0.14	9.36	-0.08	7.78	-0.01	0.36	0.08	1.72	0.11	1.95	0.02	0.18
15	6	-0.48	8.83	0.57	7.58	0.00	0.15	0.05	5.24	-0.12	4.78	-0.01	0.25	0.03	1.31	0.08	1.30	0.01	0.12
1	12	0.48	7.23	-0.40	9.38	0.22	2.61	-2.23	38.36	0.29	30.93	-0.16	3.22	1.30	9.03	-0.21	9.77	0.02	2.18
2	12	0.26	3.45	-0.10	4.02	0.08	1.20	-0.29	25.46	1.82	21.64	-0.12	1.54	0.72	4.76	-0.02	4.86	0.03	1.04
3	12	0.26	2.80	0.04	2.50	0.04	0.75	0.72	21.66	1.00	14.92	-0.08	0.97	0.44	2.94	0.02	3.19	0.02	0.65
5	12	0.15	1.44	0.00	1.45	0.01	0.44	-0.39	14.12	-0.03	8.15	-0.05	0.57	0.26	1.80	0.03	1.91	0.02	0.38
10	12	-0.02	2.44	0.00	0.71	0.00	0.21	0.41	7.39	-0.08	3.46	-0.02	0.27	0.10	1.20	0.05	0.99	0.01	0.19
15	12	-0.10	3.22	0.01	0.47	0.00	0.13	-0.04	3.52	-0.14	2.69	-0.01	0.18	0.03	1.39	0.04	0.70	0.01	0.12
1	24	-0.02	3.22	-0.10	4.58	0.00	1.85	0.06	26.49	-0.15	9.53	0.19	2.57	0.07	4.32	0.19	6.86	0.07	2.21
2	24	0.01	1.52	0.00	2.14	0.01	0.87	-0.36	14.36	-0.09	3.79	0.04	1.15	0.02	2.10	0.18	3.32	0.04	0.96
3	24	0.01	1.02	0.00	1.42	0.01	0.57	0.48	10.43	-0.09	2.46	0.02	0.76	0.02	1.41	0.11	2.19	0.03	0.60
5	24	0.01	0.62	0.00	0.86	0.01	0.33	0.03	7.26	-0.09	1.43	0.00	0.45	0.01	0.86	0.10	1.29	0.02	0.34
10	24	-0.02	0.53	0.00	0.46	0.00	0.16	0.14	3.46	-0.07	0.71	0.00	0.21	0.01	0.47	0.07	0.64	0.01	0.16
15	24	-0.01	0.37	0.00	0.30	0.00	0.10	0.01	2.12	-0.05	0.48	0.00	0.14	0.00	0.36	0.05	0.42	0.01	0.10

At $t \geq 3000$ s the vessel with the source enters geometrical shadow making SNR<1. This results in spreading sonograms $\Delta\varphi_x(t)$ and $\Delta\varphi_y(t)$, however the "ghost" phase is clearly visible in the geometrical shadow. Notable that the phase differences $\Delta\varphi_x(t)$ and $\Delta\varphi_y(t)$ of both tone and noise-shape signal have zero means all over the 3000 to 4500 s time interval. In the geometrical shadow the *x*- or *y*- channel detects diffracted signals. Vertical channel of the sensor 530 m deep does not record any tone from the source 60 m deep, see Fig. 5a.

However, the noise-shaped signal from on-water source – the research vessel – is visible, see Fig. 5b. Fig. 5a,b shows prevailing diffusive noise in $\Delta\varphi_z(t)$ sonogram at $t \geq 3000$ s. The phase difference has an even distribution in the diffusive acoustic noise field. In the diffusive field [3] the phase difference mean draws to zero over the $-\pi$ to π interval or to π over the 0 to 2π interval at considerable averaging times, T≈100 s. At the same time the standard deviation is $\sigma = 2\pi/2\sqrt{3} \approx \pm 100$ deg. As the research proves the tone or noise-shaped signal require much shorter averaging time.

4. CONCLUSIONS

Statistical analysis of the phase-difference relationship between the sound pressure $p(t)$ and the particle velocity vector $\vec{V}(t)$ might be useful while considering compound acoustic fields at short averaging times.

REFERENCES

[1] A. Zhukov, A. Ivannikov, B. Nunin, O. Tonakanov, On medium particle movement in the acoustic fields of compound structure, MSU Courier, Sect. 3, Vol.26, №2, 1985, (in Russian).

[2] V. Shchurov, Coherent and diffusive fields of underwater acoustic ambient noise, J. Acoust. Soc. Am., Vol. 90 (2), pt 1, 991–1001, 1991.

[3] V. Shchurov, Vector acoustics of the ocean, Dalnauka, 296, Vladivostok 2006.